JACS
JOURNAL OF THE AMERICAN CHEMICAL SOCIETY

Article

pubs.acs.org/JACS

Prussian Blue Nanoparticles as Multienzyme Mimetics and Reactive Oxygen Species Scavengers

Wei Zhang,[⊥,†] Sunling Hu,[⊥,†] Jun-Jie Yin,[‡] Weiwei He,[‡] Wei Lu,[§] Ming Ma,[†] Ning Gu,*[,†] and Yu Zhang*[,†]

[†]State Key Laboratory of Bioelectronics, Jiangsu Key Laboratory for Biomaterials and Devices, School of Biological Science and Medical Engineering & Collaborative Innovation Center of Suzhou Nano Science and Technology, Southeast University, Nanjing 210096, P. R. China

[‡]Division of Analytical Chemistry, Office of Regulatory Science, Center for Food Safety and Applied Nutrition, United States Food and Drug Administration, College Park, Maryland 20740, United States

[§]Department of Neurobiology, Nanjing Medical University & Key Laboratory of Developmental Genes and Human Disease, Institute of Life Sciences, Southeast University, Nanjing 210096, P. R. China

Supporting Information

ABSTRACT: The generation of reactive oxygen species (ROS) is an important mechanism of nanomaterial toxicity. We found that Prussian blue nanoparticles (PBNPs) can effectively scavenge ROS via multienzyme-like activity including peroxidase (POD), catalase (CAT), and superoxide dismutase (SOD) activity. Instead of producing hydroxyl radicals (•OH) through the Fenton reaction, PBNPs were shown to be POD mimetics that can inhibit •OH generation. We theorized for the first time that the multienzyme-like activities of PBNPs were likely caused by the abundant redox potentials of their different forms, making them efficient electron transporters. To study the ROS scavenging ability of PBNPs, a series of in vitro ROS-generating models was established using chemicals, UV irradiation, oxidized low-density lipoprotein, high glucose contents, and oxygen glucose deprivation and reperfusion. To demonstrate the ROS scavenging ability of PBNPs, an in vivo inflammation model was established using lipoproteins in Institute for Cancer Research (ICR) mice. The results indicated that PBNPs hold great potential for inhibiting or relieving injury induced by ROS in these pathological processes.

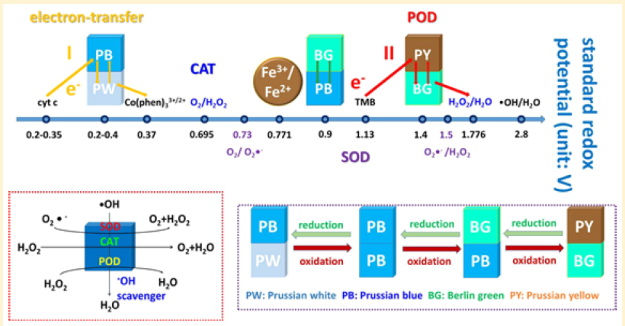

INTRODUCTION

Since Diesbach first synthesized Prussian blue (PB) in Berlin in 1706, PB has been commonly used as a dye and has been used in iron staining of biopsy specimens. PB has been used in various fields including magnetics, photology, electrochemistry, and biomedicine.[1−4] More importantly, the Food and Drug Administration (FDA) has approved PB as an antidote for thallium in 2010.[1] PB can harmlessly pass through the body due to its high binding affinity for cyanide ions. Our group initially discovered that Prussian blue nanoparticles (PBNPs) could effectively scavenge reactive oxygen species (ROS), which are thought to be implicated in many forms of apoptosis and cell death in many diseases. The ROS scavenging ability of PBNPs is attributed to their affinity for hydroxyl radicals (•OH) and their ability to mimic three antioxidant enzymes: peroxidase (POD), catalase (CAT), and superoxide dismutase (SOD) (Scheme 1a). We previously[5,6] reported that PB-modified γ-Fe_2O_3 and ferritin nanoparticles had high POD-like activity. We further discovered that PBNPs were versatile enzyme-like nanomimetics, also possessing CAT- and SOD-like activities. With these properties, PBNPs could protect cells from oxidative stress induced by cisplatin (CDDP), diallyl trisulfide (DATS), UVA irradiation, lipopolysaccharide (LPS), phorbol 12-myristate 13-acetate (PMA), high glucose contents, oxidized low density lipoprotein (OxLDL), and hypoxia-hypoglycemia and reoxygenation (HR). In addition to their cytoprotective ability, PBNPs have been shown to exert anti-inflammatory effects in animal models.

RESULTS AND DISCUSSION

Preparation and Characterization of PBNPs. The PBNPs were prepared using simple colloidal chemistry with polyvinylpyrrolidone (PVP), which is a common auxiliary material in pharmaceuticals as a stabilizer (Scheme S1).[7,8] The scanning electron microscopy (SEM) (Figure S1a) and transmission electron microscopy (TEM) images (Figure S1b) show that the synthesized PBNPs are cubic particles with an average size of about 50 nm. The particles have a crystalline structure with strong and typical diffraction spots.

Received: November 20, 2015
Published: February 26, 2016

DOI: 10.1021/jacs.5b12070
J. Am. Chem. Soc. 2016, 138, 5860−5865

Scheme 1. (a) Schematic Diagram Showing Intracellular Behaviors of PBNPs in Vitro. (b) Schematic Mechanism of the Multienzyme-like Activity of PBNPs Based on Standard Redox Potentials of Different Compounds in the Reaction Systems

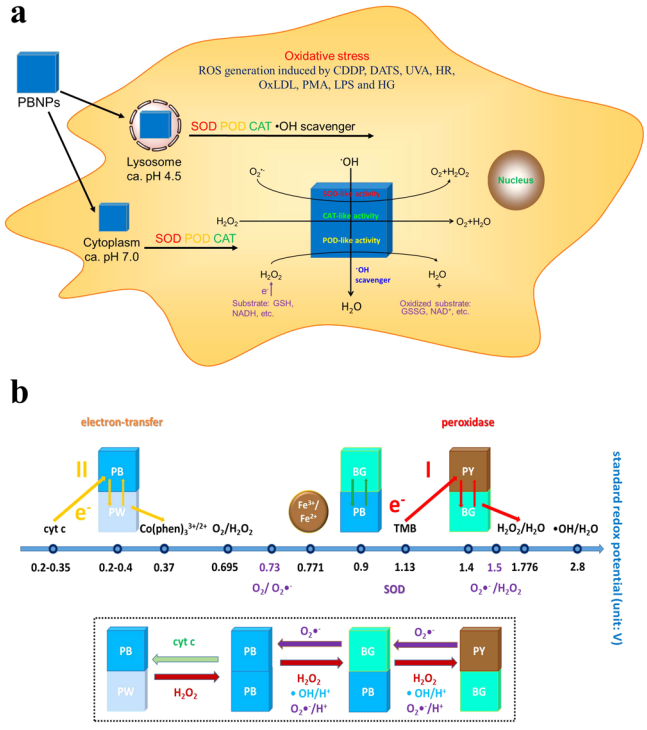

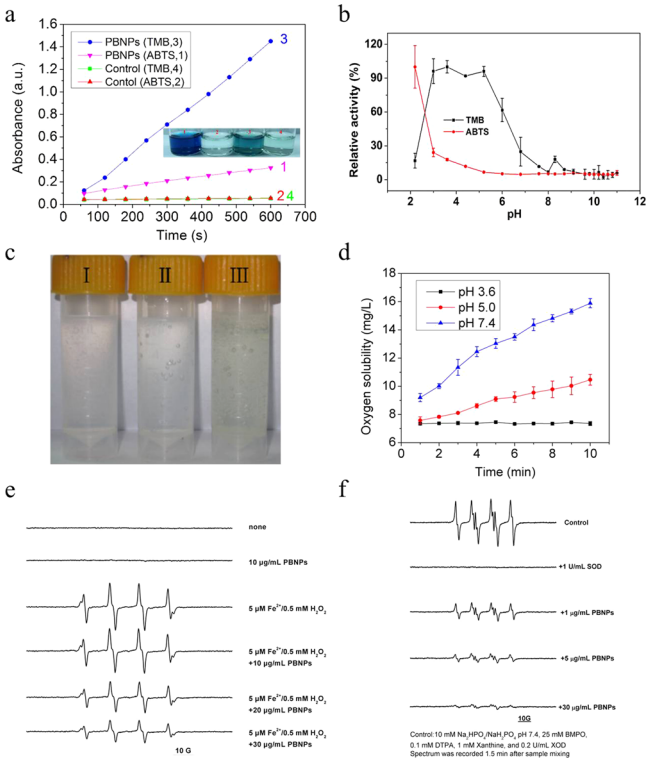

Figure 1. (a) PBNPs show POD-like activity. (b) The curve of the POD-like activity of PBNPs versus pH. (c) Images of systems reacting for 4 min at pH 7.4: (I) pure H_2O_2, (II) 0.25 μg/mL PBNPs and 1.2 mM H_2O_2, (III) 0.25 μg/mL PBNPs, 1.2 mM H_2O_2, and 0.4 mg/mL TMB. (d) Oxygen generation catalyzed by PBNPs increased gradually with time at pH 3.6 (black line), 5.0 (red line), and 7.4 (blue line). (e) The effect of PBNPs on •OH from Fenton reagents at pH 3.9. The signal intensities of the second line in the spectrum of BMPO/•OH are 925, 856, 594, and 430 au, respectively. (f) Change in DMPO/•OOH ESR signal upon addition of SOD or PBNPs.

The calculated d spaces are 0.49 nm for (200), 0.35 nm for (220), and 0.25 nm for (400) (Figure S1c). PBNPs can be well dispersed in water with an average hydrodynamic diameter of 92.93 nm and a polydispersity index (PDI) of 0.092 (Figure S1d). The UV−vis absorption spectrum of PBNPs shows an obvious characteristic peak of PB at approximately 700 nm (Figure S1e), which can be attributed to the intermetallic charge-transfer band from Fe^{2+} to Fe^{3+} in PB.[9,10] The PBNPs exhibited a Fourier transform infrared spectroscopy (FTIR) absorption peak at 2090 cm^{-1}, which is characteristic of CN stretching in the Fe^{2+}−CN−Fe^{3+} bond of PB,[11,12] and a peak at 1670 cm^{-1}, indicative of C═O stretching in the PVP amide unit, which is consistent with that of pure PVP (Figure S1f).[13,14]

POD- and CAT-like Activities of PBNPs. Commonly used natural POD substrates, 3,5,3′,5′-tetramethylbenzidine (TMB) and 2,2′-azino-di(3-ethylbenzthiazoline-6-sulfonic acid) (ABTS), were selected as substrates to investigate the POD activity of PBNPs (Figure 1a). The steady-state kinetic behavior was investigated at room temperature, and the resulting curves followed the Michaelis−Menten equation (Figure S2). On the basis of the calculated kinetic parameters (Table S1), the k_{cat} values (1.16×10^5) of PBNPs were higher than those of Fe_3O_4 NPs (3.02×10^4 with TMB as a substrate),[15] indicating that PBNPs had higher POD-like activity. The K_m value of PBNPs using TMB as a substrate was higher than that for ABTS, suggesting that PBNPs had a greater affinity for TMB than ABTS. This result was likely due to the negative zeta potential of PBNPs (−26.1 mV). In fact, PBNPs have similar properties to natural enzymes, that is, the POD-like activity increased with concentration and was dependent on temperature (Figure S3) and pH (Figure 1b).

It is noteworthy that PBNPs showed weak POD activity under neutral conditions. In an alkaline environment, they were nearly inactive; instead, observable bubbles show up in the solution (Figure 1c). By using a dissolved oxygen electrode, the gas generated was verified to be O_2, which gradually increased with time at higher pH levels (Figure 1d). An oximetry method (Figure S4) was used to detect the O_2 generation rate (Figure S5a). We demonstrated that the CAT-like activity of PBNPs was linearly dependent on the concentration of PBNPs. Remarkably, under higher pH levels, the oxygen solubility increased with PBNP concentration (Figure S5b). The reaction mechanism between iron-based nanoparticles and H_2O_2 is typically modeled after the Fenton reaction; the resultant •OH molecules induce biotoxicity.[5,15] Initially, we hypothesized that the catalytic reaction mechanism of PBNPs also followed the Fenton reaction. However, no apparent BMPO/•OH signal was observed in the H_2O_2 solution regardless of the presence of PBNPs (Figure 1e, second line). Furthermore, the Fenton reaction (Figure 1e, third line) was triggered using the Fe^{2+}/H_2O_2 system to produce •OH at pH 3.9. Surprisingly, the electron spin resonance (ESR) signal of BMPO/•OH decreased with increasing PBNP concentration. This result could be attributed to either Fe^{2+} chelation or scavenging of the produced •OH. A TiO_2/UV system (Figure S6) that produced

DOI: 10.1021/jacs.5b12070
J. Am. Chem. Soc. 2016, 138, 5860−5865

•OH (final pH was approximately 4.5)[16] was used to investigate the actual effect of PBNPs on hydroxyl radicals. The signal intensity of DMPO/•OH decreased dramatically as the concentration of PBNPs increased, which suggested a direct •OH scavenging capability of PBNPs in acidic environments. This effect may be due to the reducing ability of PBNPs and low redox potential. In general, PB can be reduced into Prussian White (PW) and oxidized into Berlin Green (BG) or Prussian Yellow (PY) via reactions 1, 2, and 3. The redox potentials of PB/PW, BG/PB, and PY/BG are 0.2−0.4, 0.9, and 1.4 V, respectively, at pH 3.0−8.0.[12,17−20] These compounds gradually and continuously changed along with the redox potential of the environment. The reduction of •OH by PBNPs is represented in reaction 4.

$[Fe(III)Fe(II)(CN)_6]^-$ (PB)

$[Fe(II)Fe(II)(CN)_6]^{2-}$ (PW)

$\{Fe(III)_3[Fe(III)(CN)_6]_2[Fe(II)(CN)_6]\}^-$ (BG)

$[Fe(III)Fe(III)(CN)_6]$ (PY)

$$PB + e^- \rightarrow PW \quad (1)$$

$$3PB \rightarrow BG + 2e^- \quad (2)$$

$$PB \rightarrow PY + e^- \quad (3)$$

$$PB + H^+ + \bullet OH \rightarrow PY + H_2O \quad (4)$$

$$H_2O_2 \rightarrow O_2 + 2e^- + 2H^+ \quad (5)$$

$$H_2O_2 + 2e^- + 2H^+ \rightarrow 2H_2O \quad (6)$$

$$TMB + H_2O_2 + 2H^+ \xrightarrow{PY} TMB\ (oxidized) + 2H_2O \quad (7)$$

It was reported that H_2O_2 can be oxidized or reduced through two electron transfer channels in PB, high-spin $Fe^{3+/2+}$ and low-spin $Fe(CN)_6^{3-/4-}$ (reactions 5 and 6),[18] respectively. When the electrode potential is lower than 0.7 V, the electron transfer of high-spin $Fe^{3+/2+}$ plays the main role. When the electrode potential reaches 0.9 V, the low-spin system $[Fe(CN)_6]^{3-/4-}$ is predominant. The oxidation and reduction of H_2O_2 can be illustrated according to the theoretical redox potential of different redox couples in the reaction systems. The standard redox potentials of an O_2/H_2O_2 couple and an H_2O_2/H_2O couple are 0.695 and 1.776 V, respectively (all standard redox potentials are listed[21−29] in Scheme 1b). H_2O_2 possesses strong oxidation characteristics in acidic environments. Reaction 6 and the oxidation of PBNPs into BG or PY are more likely to occur at pH 3.6 than at pH 7.4. As a result, at a suitable potential (1.4 V), PY/BG can transfer electrons from TMB (TMB^{Ox}/TMB^{Re} 1.13 V) to H_2O_2 (H_2O_2/H_2O 1.776 V) (Scheme 1b, I) and primarily contributes to the POD-like activity of PBNPs as shown in reaction 7. The standard redox potential of Fe^{3+}/Fe^{2+} is at most 0.771 V. Electrons from TMB cannot pass through iron oxide nanoparticles (IONPs, a typical representative of iron-based nanoparticles) to H_2O_2. Therefore, the oxidation of TMB is primarily induced by the Fenton reaction-formed •OH.[30] To further verify the POD-like activity mechanism of PBNPs, a cytochrome c (cyt c, electron donor, 0.2−0.35 V)/phenanthroline cobalt ($Co(phen)_3^{3+}$, electron acceptor, 0.37 V) system[31] was established to determine the role of PBNPs in the electron transfer procedure (Scheme 1b, II). The reduction state of cyt c (in pH 3.6 buffer) is characterized by the Soret peak at 410 nm due to the presence of porphyrin chromophore and two small peaks at 520 and 550 nm. When oxidized, the Soret peak fades, the two peaks at 520 and 550 nm disappear, and a small peak at 530 nm is observed. The UV−vis spectra (Figure S7a) have matched absorption peaks of reduced cyt c at approximately 520 and 550 nm and oxidized cyt c at 530 nm,[32,33] indicating that the PBNPs act as electron transfer agents to efficiently accelerate the oxidation of cyt c by $Co(phen)_3^{3+}$; PBNPs themselves do not oxide cyt c. PB is known to be unstable under alkaline conditions.[18] The stability of PBNPs at different pH levels was studied (Figure S8a,b). PBNPs were stable for at least 20 min (Figure S7b) at pH 3.6 and 7.4. The decreased absorbance at 700 nm within 20 min (Figure S7c) shows the oxidation of PBNPs rather than the decomposition of PBNPs. At higher pH, the redox potential of H_2O_2/O_2 is very low, and H_2O_2 can be more easily oxidized into O_2. Hence, fewer PBNPs were oxidized into BG or PY, which can transfer electrons from TMB to H_2O_2 (Figure S7c). Therefore, the POD-like activity of PBNPs was very weak at higher pH levels. Under these conditions, CAT-like activity, as described by reactions 8−11, plays a major role:

$$3PB + H_2O_2 \rightarrow BG + 2OH^- \quad (8)$$

$$2BG + H_2O_2 \rightarrow 6PY + 2OH^- \quad (9)$$

$$6PY + H_2O_2 + 2OH^- \rightarrow 2BG + O_2 + 2H_2O \quad (10)$$

$$BG + H_2O_2 + 2OH^- \rightarrow 3PB + O_2 + 2H_2O \quad (11)$$

SOD-like Activity of PBNPs. From the ESR results (Figure 1f, Figure S9), we identified PBNP SOD mimetics that effectively quenched superoxide radicals ($O_2\bullet^-$) at different pH levels. Superoxides were generated using the xanthine/xanthine oxidase system. BMPO was used as a spin trap to form BMPO/•OOH. The ESR spectrum can be decreased by SOD or PBNPs at different pH levels. The BMPO/•OOH signal decreased with increasing PBNP concentration, suggesting that PBNPs displayed SOD-like activity. We infer that the mechanism for these phenomena obeys reaction 12. H_2O_2 can be transformed into H_2O or O_2 by PBNPs acting as POD- or CAT-like nanoenzymes. The standard redox potential values of $O_2/O_2\bullet^-$ (0.73 V) and $O_2\bullet^-/H_2O_2$ (1.5 V) indicate that the PBNPs are capable of catalyzing half-reactions 13−16. The PBNP-catalyzed dismutation of $O_2\bullet^-$ utilizes the same mechanism as SOD:

$$2 \bullet OOH \xrightarrow{SOD/PBNPs} H_2O_2 + O_2 \quad (12)$$

$$2 \bullet OOH + 2H^+ + 3PB \rightarrow 2H_2O_2 + BG \quad (13)$$

$$2 \bullet OOH + BG \rightarrow 2O_2 + 2H^+ + 3PB \quad (14)$$

$$\bullet OOH + H^+ + BG \rightarrow H_2O_2 + 3PY \quad (15)$$

$$\bullet OOH + 3PY \rightarrow O_2 + H^+ + BG \quad (16)$$

PBNPs Protect Cells against Oxidative Stress in Vitro. PBNPs were stable in physiological solutions, without obvious changes in hydrodynamic size during 7 days of incubation (Figure S8c). Observations of cell morphology and anchorage-dependent rates (Figure S10A) revealed that PBNPs did not affect cell growth or morphology. MTT cell viability results (Figure S10B) indicated that PBNPs had almost no cytotoxicity. The cell viability was consistent over various concentrations of PBNPs. Furthermore, the PBNPs had no

DOI: 10.1021/jacs.5b12070
J. Am. Chem. Soc. 2016, 138, 5860−5865

differential effects on different cell types including HUVECs (human umbilical vein endothelial cells), RAW264.7 (mouse macrophages), HBZY-1 (rat glomerulus mesangial cells), NIH-3T3 (mouse fibroblast cells), and HT (hippocampal neural cells) cells. TEM images (Figure S10) showed that PBNPs localized to lysosomes (pH 4.5[30,34]) and the cytosol (pH 7.0), demonstrating that PBNPs were taken up by RAW264.7 and HBZY-1 cells. In different intracellular microenvironments, PBNPs may exert differential enzyme-like activities. PBNPs mainly function as SOD mimetics, high-activity CAT mimetics, and low-activity POD mimetics when distributed in the cytosol. In lysosomes, PBNPs also act at •OH scavengers and have stronger POD-like activity and weaker CAT-like activity. PBNPs may be able to protect cells from ROS-induced cytotoxicity by scavenging •OH, $O_2•^-$, and H_2O_2. As shown in Figure S12, iron contents of cells were detected using inductively coupled plasma optical emission spectroscopy (ICP-OES), and the results indicated that the cellular uptake of PBNPs was dose-dependent. HBZY-1 cells were used to study the protective actions of PBNPs against kidney damage induced by CDDP, which has been used as a first-line drug against tumors in the past few decades. The IC_{50} (half maximal inhibitory concentration) value for 48 h of CDDP treatment of HBZY-1 cells was 42.1 μM (Figure S13a). As seen in Figure 2,

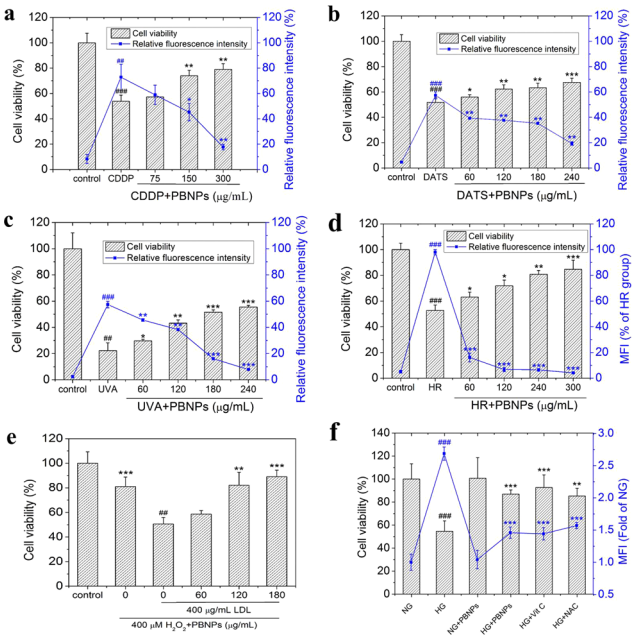

Figure 2. PBNPs can protect cells from oxidative stress induced by (a) CDDP, (b) DATS, (c) UVA irradiation, (d) HR, (e) OxLDL, and (f) HG via ROS scavenging. Graphs show means and s.e.m. Symbols indicate the relative level of significance compared with the control group (##, $p < 0.01$ and ###, $p < 0.001$) or with the oxidative stress model groups (∗, $p < 0.05$; ∗∗, $p < 0.01$; ∗∗∗, $p < 0.001$), Student's t test.

panel a, 40 μM CDDP had a remarkable cytotoxicity after 48 h in vitro ($p < 0.001$) with significant ROS generation ($p < 0.01$). However, 150 μg/mL of PBNPs effectively inhibited the ROS generation ($p < 0.05$) and increased the cell viability ($p < 0.01$). On the basis of these results, PBNPs could be considered to potentially inhibit the nephrotoxicity of CDDP.

In fact, PB is an FDA-approved drug for the treatment of thallotoxicosis because thallium (Tl) can replace potassium in PB and form insoluble products, which are then excreted in feces.[35] Similar to CDDP, the Tl influx in cells is mediated by Na−K-ATPase and may increase ROS generation in cells, likely via the same mechanism.[36,37] Furthermore, the affinity for sulfhydryl groups of endogenous glutathione (GSH) importantly explains why Tl may induce ROS production. We provide definitive evidence that PBNPs can effectively inhibit ROS production induced by CDDP and reduce the cytotoxicity of CDDP in HBZY-1 cells. The ROS scavenging ability of PBNPs is likely another reason for their use as an antidote for thallium. DATS induces ROS production in cells and is widely used to kill tumor cells.[38] Our results showed that DATS also induces cytotoxicity in HUVECs and has an IC_{50} value of 26.5 μM (Figure S13b). Pretreatment with 60 μg/mL of PBNPs effectively attenuates DATS-induced intracellular ROS production ($p < 0.01$) and increases cell viability ($p < 0.05$) (Figure 2b). Using NIH-3T3 cells, we showed that 60 μg/mL of PBNPs reduced the production of UVA-induced ROS ($p < 0.01$, Figure 2c) and decreased UVA-induced apoptosis ($p < 0.05$). These results are independent of the so-called "sunscreen" effect because within the concentrations used, PBNPs do not exhibit any absorbance at 365 nm. An oxygen and glucose deprivation/reperfusion (HR) model of HT cells was established to study the inhibiting effects of PBNPs on the HR-induced apoptosis of nerve cells. We observed that PBNPs obviously inhibited ROS production in HT cells under HR ($p < 0.001$, Figure 1d). MTT assays indicated that PBNPs significantly increased the number of live HT cells ($p < 0.05$) and that the cell survival rate was approximately 52.7% under 24 h of normal oxygen conditions after the cells were subjected to hypoxic conditions for 1 h. A 60 μg/mL of PBNP treatment efficiently protected HT cells (cell viability up to 63.1%), likely by inhibiting ROS production ($p < 0.001$). These results indicate that PBNPs may play a protective role against neuron injury induced by HR. A Human OxLDL ELISA Kit (CUSABIO, Wuhan, Hubei Province, P.R.China) was used to detect OxLDL in the PBNP-incubated samples. Remarkably, PBNPs efficiently reduced the generation of OxLDL due to their ROS scavenging activity (Figure S14). An oxidative damage model was established by culturing PIECs (pig iliac endothelial cells) with OxLDL in vitro. Treatments with 120 μg/mL of PBNPs effectively inhibited cell deactivation induced by OxLDL ($p < 0.01$, Figure 2e). Our research demonstrates that PBNPs are effective scavengers of ROS and suppress lipid peroxidation, as shown by protecting PIECs from oxidation damage. Glucose has been considered a factor that induces cell death through a free radical-mediated mechanism.[39] In diabetes patients, increased oxidative stress and hyperglycemia can directly lead to the overproduction of ROS. As shown in Figure 2, panel f, the exposure of cultured HUVECs to high glucose (HG) conditions for 72 h induced a significant increase in ROS compared with cells exposed to normal glucose (NG) conditions ($p < 0.001$). This result suggests a stimulatory effect of HG on ROS production. When pretreated with 1 mM PBNPs, 1 mM vitamin C (Vit C), or 1 mM N-acety-L-cysteine (NAC) for 24 h, the intracellular ROS content decreased ($p < 0.001$). The PBNPs themselves did not influence the ROS content in HUVECs cultured under NG conditions. The results in Figure 2, panel f show that PBNPs, Vit C, and NAC all effectively improved the cell viability of HUVECs under HG conditions ($p < 0.01$).

Anti-inflammatory Effect of PBNPs in Vitro and in Vivo. Respiration bursts occur in macrophages under

DOI: 10.1021/jacs.5b12070
J. Am. Chem. Soc. 2016, 138, 5860−5865

stimulation. ROS production is accompanied by respiration bursts and damages adjacent cells, causing inflammation such as arthritis. PMA and LPS can increase inflammation in macrophages.[40,41] We used a well-defined model of macrophage activation at inflammatory sites by treating RAW264.7 cells with LPS/PMA to increase ROS production (Figure S15). Cells that were treated with 10 ng/mL of LPS for 48 h underwent dramatic morphological changes characterized by hypertrophy and extensive vacuolization (Figure 3A, b,f). By using the endogenous antioxidant GSH (Figure 3A, d,h), PBNPs can effectively protect RAW264.7 cells from damage by LPS (Figure 3A c,g, $p < 0.001$ in Figure S15). Table S2 and Figure S16 show that the hemolysis rate of PBNPs was less than 1%, which is well within the permissible limits of ISO 10993−4 standards, that is, PBNPs can be used for injections. Figure S17 illustrates the distribution of PBNPs in Institute for Cancer Research (ICR) mice 1 week after treatment by intravenous injections of 20 mg/kg of PBNPs. PBNPs accumulated in the liver and spleen along with many phagocytes. The biodistribution of iron was quantified by ICP-OES 24 h and 7 d postinjection. PBNPs mainly accumulated in the liver and spleen (Figure 3B, a). Because of the distribution of PBNPs in the liver, we further investigated the in vivo feasibility of using PBNPs to inhibit oxidative stress in mice liver inflammation models. These in vivo studies showed that PBNPs could protect the body from oxidative damage and slow down the inflammatory response. The liver tissues of LPS-treated mice (Figure 3C, b) showed focal nuclear pyknosis, inflammatory cell infiltration, and even bile stasis (yellow part), that is, cholestasis, which demonstrates that LPS can simulate mouse acute hepatitis. In PBNP-pretreated mice, almost no histological alterations in the liver were observed compared with the control mice. The cellular space may be induced by the production of oxygen from the CAT-like activity of PBNPs. Quantitative analyses showed that the number of TUNEL-positive cells was markedly decreased in the PBNP-pretreated group compared with the LPS group (1.01% ± 0.81% vs 9.12% ± 2.14% as shown in Figure 3D). ROS levels in liver were measured to determine the oxidative stress status. Alanine transaminase (ALT), interleukin sera (IL)-6 and IL-8 were used to assess the inflammation status. The results show that LPS can stimulate ROS production in liver tissue ($p < 0.001$) and that PBNPs can reduce or event prevent this production ($p < 0.01$, Figure 3B, b). As shown in Figure S18, LPS increased ALT ($p < 0.001$), an enzyme mainly related to hepatocytes in the liver, indicating the extent of hepatocyte damage. The preinjection of PBNPs effectively inhibited ROS increase ($p < 0.001$). PBNPs accumulated in the liver and protected hepatocytes from damage. The up-regulation of IL-6 ($p < 0.001$) and IL-8 ($p < 0.01$) signaled inflammation in the LPS group. The low levels in the PBNPs + LPS group ($p < 0.01$) indicated the ability of PBNPs to inhibit inflammation.

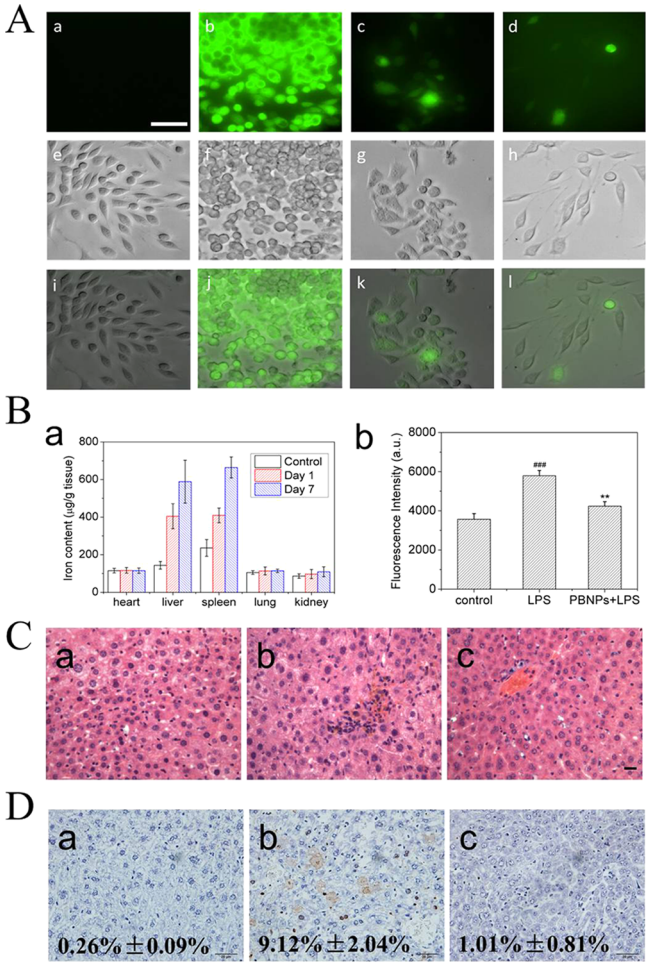

Figure 3. PBNPs can inhibit ROS generation induced by LPS. (A) Fluorescence microscopic images (a−d), bright-field microscopic images (e−h), and merged images (i−l) of RAW264.7 cells. (a) Normal RAW264.7 cells; (b) RAW264.7 cells were stimulated by LPS; (c) RAW264.7 cells were preincubated with PBNPs then stimulated by LPS; (d) RAW264.7 cells were preincubated with GSH and then stimulated LPS. Scale bar, 200 μm. (B) In vivo accumulation of PBNPs in mice (a) and ROS intensities in liver tissues (b). Time-dependent biodistribution measurement of iron levels in various organs including heart, liver, spleen, lung, and kidneys of mice after double injection of 20 mg/kg of PBNPs, using 0.9% saline injected ICR mice as control. The second injection was carried out on the fourth day. ROS intensities were measured in liver tissues of the same mass excised from control mice, LPS-treated mice, and LPS-treated mice with 1 week chronic injection of PBNPs. ROS intensity was expressed by fluorescence intensity; bars represent the means ± s.e.m. ($n = 5$). ### indicates $p < 0.001$ compared with the control group; ** indicates $p < 0.01$ compared with the LPS group. (C) Hematoxylin and Eosin (H&E) staining images of liver histology. Liver tissues were excised from (a) control, (b) LPS-treated mice, and (c) LPS-treated mice with 1 week preinjection of PBNPs. Scale bar, 20 μm. (D) TUNEL staining images of mice liver tissue sections from (a) control, (b) LPS-treated mice, and (c) LPS-treated mice with 1 week preinjection of PBNPs.

CONCLUSIONS

In this study, we demonstrated the ability of PBNPs to mimic POD, CAT, and SOD likely caused by their abundant redox potentials in different forms including PB, PW, BG, and PY, which made them strong electron transporters. Many nanoparticles are harmful in biological systems and have the potential to generate toxic effects by producing ROS. However, ESR results have shown that PBNPs, unlike other iron-based nanoparticles, can inhibit the production of •OH. Our results show that PBNPs can also efficiently quench $O_2•^-$ and H_2O_2, which make PBNPs nanosized ROS scavengers. These findings may shed new light on the mechanisms and applications of mimetic enzymes. PBNPs have the potential to become potent antioxidants for controlling ROS-induced cell damage. Our results verified that PBNPs have ROS scavenging abilities in

DOI: 10.1021/jacs.5b12070
J. Am. Chem. Soc. 2016, 138, 5860−5865

several cell models. However, the detailed cellular mechanism of this property of PBNPs requires further studies.

■ ASSOCIATED CONTENT

Supporting Information

The Supporting Information is available free of charge on the ACS Publications website at DOI: 10.1021/jacs.5b12070.

Experimental details, figures, and tables (PDF)

■ AUTHOR INFORMATION

Corresponding Authors

*zhangyu@seu.edu.cn

*guning@seu.edu.cn

Author Contributions

⊥These authors contributed equally.

Notes

The authors declare no competing financial interest.

■ ACKNOWLEDGMENTS

This research was supported by the National Basic Research Program of China (Nos. 2011CB933503, 2013CB733800), the National Natural Science Foundation of China (Nos. 31170959, 81571806), the Basic Research Program of Jiangsu Province (No. BK2011036), the Jiangsu Provincial Technical Innovation Fund for Scientific and Technological Enterprises (No. SBC201310643), and the Jiangsu Provincial Special Program of Medicine Science (BL2013029). This work was partially supported by a regulatory science grant under the FDA Nanotechnology CORES Program. This article is not an official U.S. FDA guidance or policy statement. No official support or endorsement by the U.S. FDA is intended or should be inferred.

■ REFERENCES

(1) Jing, L.; Liang, X.; Deng, Z.; Feng, S.; Li, X.; Huang, M.; Li, C.; Dai, Z. *Biomaterials* **2014**, *35*, 5814.

(2) Yang, F.; Hu, S.; Zhang, Y.; Cai, X.; Huang, Y.; Wang, F.; Wen, S.; Teng, G.; Gu, N. *Adv. Mater.* **2012**, *24*, 5205.

(3) Larionova, J.; Guari, Y.; Sangregorio, C.; Guérin, C. *New J. Chem.* **2009**, *33*, 1177.

(4) Su, L.; Xiong, Y.; Yang, H.; Zhang, P.; Ye, F. *J. Mater. Chem. B* **2016**, *4*, 128.

(5) Zhang, X.-Q.; Gong, S.-W.; Zhang, Y.; Yang, T.; Wang, C.-Y.; Gu, N. *J. Mater. Chem.* **2010**, *20*, 5110.

(6) Zhang, W.; Zhang, Y.; Chen, Y.; Li, S.; Gu, N.; Hu, S.; Sun, Y.; Chen, X.; Li, Q. *J. Nanosci. Nanotechnol.* **2013**, *13*, 60.

(7) Yen, F.-L.; Wu, T.-H.; Tzeng, C.-W.; Lin, L.-T.; Lin, C.-C. *J. Agric. Food Chem.* **2010**, *58*, 7376.

(8) Sharma, D.; Chelvi, T. P.; Kaur, J.; Chakravorty, K.; De, T. K.; Maitra, A.; Ralhan, R. *Oncol. Res.* **1995**, *8*, 281.

(9) Pyrasch, M.; Tieke, B. *Langmuir* **2001**, *17*, 7706.

(10) Zhao, W.; Xu, J.-J.; Shi, C.-G.; Chen, H.-Y. *Langmuir* **2005**, *21*, 9630.

(11) Mee Jung, Y.; Park, Y.; Sarker, S.; Lee, J.-J.; Dembereldorj, U.; Joo, S.-W. *Sol. Energy Mater. Sol. Cells* **2011**, *95*, 326.

(12) Ellis, D.; Eckhoff, M.; Neff, V. *J. Phys. Chem.* **1981**, *85*, 1225.

(13) Jiang, T.; Xu, K. *Carbon* **1995**, *33*, 1663.

(14) Uemura, T.; Kitagawa, S. *J. Am. Chem. Soc.* **2003**, *125*, 7814.

(15) Gao, L.; Zhuang, J.; Nie, L.; Zhang, J.; Zhang, Y.; Gu, N.; Wang, T.; Feng, J.; Yang, D.; Perrett, S.; et al. *Nat. Nanotechnol.* **2007**, *2*, 577.

(16) Wamer, W. G.; Yin, J.-J.; Wei, R. R. *Free Radical Biol. Med.* **1997**, *23*, 851.

(17) Karyakin, A. A. *Electroanalysis* **2001**, *13*, 813.

(18) Koncki, R. *Crit. Rev. Anal. Chem.* **2002**, *32*, 79.

(19) Zhao, G.; Feng, J.-J.; Zhang, Q.-L.; Li, S.-P.; Chen, H.-Y. *Chem. Mater.* **2005**, *17*, 3154.

(20) Itaya, K.; Uchida, I.; Neff, V. D. *Acc. Chem. Res.* **1986**, *19*, 162.

(21) Haber, F.; Weiss, J. *Proceedings of the Royal Society of London A: Mathematical, Physical, and Engineering Sciences*; The Royal Society: London, 1934.

(22) Battistuzzi, G.; Borsari, M.; Cowan, J. A.; Ranieri, A.; Sola, M. *J. Am. Chem. Soc.* **2002**, *124*, 5315.

(23) Churg, A.; Warshel, A. *Biochemistry* **1986**, *25*, 1675.

(24) Wherland, S.; Gray, H. B. *Proc. Natl. Acad. Sci. U. S. A.* **1976**, *73*, 2950.

(25) Farina, R. D.; Wilkins, R. G. *Inorg. Chem.* **1968**, *7*, 514.

(26) Cummins, D.; Gray, H. B. *J. Am. Chem. Soc.* **1977**, *99*, 5158.

(27) Dong, J.; Song, L.; Yin, J.-J.; He, W.; Wu, Y.; Gu, N.; Zhang, Y. *ACS Appl. Mater. Interfaces* **2014**, *6*, 1959.

(28) Heckert, E. G.; Karakoti, A. S.; Seal, S.; Self, W. T. *Biomaterials* **2008**, *29*, 2705.

(29) Maricle, D.; Hodgson, W. *Anal. Chem.* **1965**, *37*, 1562.

(30) Chen, Z.; Yin, J.-J.; Zhou, Y.-T.; Zhang, Y.; Song, L.; Song, M.; Hu, S.; Gu, N. *ACS Nano* **2012**, *6*, 4001.

(31) Carver, A. M.; De, M.; Bayraktar, H.; Rana, S.; Rotello, V. M.; Knapp, M. J. *J. Am. Chem. Soc.* **2009**, *131*, 3798.

(32) Jiang, X.; Jiang, J.; Jin, Y.; Wang, E.; Dong, S. *Biomacromolecules* **2005**, *6*, 46.

(33) Mukhopadhyay, A.; Joshi, N.; Chattopadhyay, K.; De, G. *ACS Appl. Mater. Interfaces* **2012**, *4*, 142.

(34) Holopainen, J. M.; Saarikoski, J.; Kinnunen, P. K.; Järvelä, I. *Eur. J. Biochem.* **2001**, *268*, 5851.

(35) Rusyniak, D. E.; Kao, L. W.; Nanagas, K. A.; Kirk, M. A.; Furbee, R. B.; Brizendine, E. J.; Wilmot, P. E. *J. Toxicol., Clin. Toxicol.* **2003**, *41*, 137.

(36) Pourahmad, J.; Eskandari, M. R.; Daraei, B. *Environ. Toxicol.* **2010**, *25*, 456.

(37) Eskandari, M. R.; Pourahmad, J.; Daraei, B. *Toxicol. Environ. Chem.* **2011**, *93*, 145.

(38) Filomeni, G.; Aquilano, K.; Rotilio, G.; Ciriolo, M. R. *Cancer Res.* **2003**, *63*, 5940.

(39) Cosentino, F.; Eto, M.; De Paolis, P.; van der Loo, B.; Bachschmid, M.; Ullrich, V.; Kouroedov, A.; Gatti, C. D.; Joch, H.; Volpe, M. *Circulation* **2003**, *107*, 1017.

(40) Roh, E.; Lee, H.-S.; Kwak, J.-A.; Hong, J. T.; Nam, S.-Y.; Jung, S.-H.; Lee, J. Y.; Kim, N. D.; Han, S.-B.; Kim, Y. *J. Infect. Dis.* **2011**, *203*, 1012.

(41) Kim, J.; Kong, C.-S.; Pyun, S. Y.; Kim, S.-K. *Carbohydr. Res.* **2010**, *345*, 1851.

DOI: 10.1021/jacs.5b12070
J. Am. Chem. Soc. 2016, 138, 5860−5865